Atmospheric tides in a Mars general circulation model with data assimilation

Atmospheric tides in a Mars general circulation model with data assimilation

S. R. Lewis [1] , P. R. Barker

Atmospheric, Oceanic and Planetary Physics, Department of Physics, University of Oxford, Clarendon Laboratory, Parks Road, Oxford OX1 3PU, United Kingdom

Abstract

The prominence of thermal tides in the Martian atmosphere has long been recognized, through classical theory, models and observations, including surface pressure records from the Viking and Mars Pathfinder Landers. A unique record of observations over more than two Martian years is now available from the Mars Global Surveyor spacecraft, although since the spacecraft is Sun-synchronous it is difficult to extract information about many tidal modes directly. Data assimilation is a technique by which observations may be combined with a Mars general circulation model (MGCM) to produce a consistent, time-evolving global analysis. Thermal and total dust opacity measurements derived from the Thermal Emission Spectrometer have been assimilated into the Oxford MGCM and the tidal modes analysed from the model surface pressure record produced by this process. Periods around regional and global dust storm events show strong, characteristic tidal signatures in the assimilations.

Key words: Mars, atmospheric tides, data assimilation

1 Introduction

Thermal tides are atmospheric modes forced by solar heating, with periods which are harmonics of the solar day. Classical theory (Chapman and Lindzen, 1970; Lindzen, 1970) describes linearized disturbances and has been applied to Mars and to Venus, as well as to the Earth. Thermal tides are particularly prominent in the Martian atmosphere owing to the strong solar forcing per unit mass (e.g. Conrath, 1976; Zurek, 1976; Zurek et al., 1992).

The direct atmospheric response to solar forcing is in Sun-synchronous components, primarily westward-propagating zonal wavenumbers one and two: the diurnal and semidiurnal tides. The semidiurnal tide has a long vertical wavelength ($\sim 100\,\mathrm{km}$)

[1] Now at: Department of Physics and Astronomy, The Open University, Walton Hall, Milton Keynes MK7 6AA, United Kingdom

and its amplitude is thought to be a good measure of the total thermal tide forcing (Zurek, 1981). This conclusion is supported by linear theory (Zurek and Leovy, 1981) and by modelling results (Wilson and Hamilton, 1996; Bridger and Murphy, 1998). Results in this paper demonstrate how closely the semidiurnal tidal amplitude is related to the atmospheric dust content, and hence to atmospheric heating by absorption of visible solar radiation.

Surface variations, in topographic height and also in thermal properties, can interact with the solar forcing to generate additional components which do not have constant phase with respect to the Sun (Conrath, 1976; Zurek, 1976; Forbes et al., 2002). One important example is the combination of the diurnal tide and zonal wavenumber two topographic variations, which gives rise to an eastward-propagating wavenumber one with a period of one day. On Mars this mode primarily takes the form of a wavenumber one Kelvin wave, which may be resonantly excited (Zurek, 1976, 1988), and which has been identified in spacecraft data (Wilson, 2000, 2002; Banfield et al., 2003). Other modes also present include modulations to the zonal-mean flow, and a semidiurnal eastward propagating mode, but these are not discussed further in the present paper.

Hess et al. (1977) and Leovy (1981) have analysed Viking Lander observations to show the presence of tidal modes on Mars. Wilson and Hamilton (1996), Bridger and Murphy (1998) and Lewis and Read (2003) describe major tidal modes found in Martian general circulation models (MGCMs). These MGCM analyses benefit from the availability of regularly-sampled, global model output, in contrast to the tidal records obtained from observations at fixed locations, as from the Viking Landers. In the case of the individual *in situ* observations it is not possible to separate the various eastward and westward propagating modes. Despite the inherent difficulty in comparing fixed point and global MGCM data, even limited surface pressure observations would have been valuable for the validation of model results. Regrettably, no local surface pressure measurements are available to coincide with the period of the Mars Global Surveyor orbiter remotely-sensed atmospheric observations used for the study here.

Figure 1 illustrates the presence of tidal modes in an MGCM simulation, using surface pressure data averaged over a northern hemisphere late autumn period under typical, non-dust storm conditions. Surface pressure along an equatorial row, sampled twelve times per day, is Fourier transformed in both longitude and time to produce a frequency–wavenumber diagram, with the amplitudes of the surface pressure modes normalised by the time-averaged surface pressure. This diagram is typical of an atmosphere with low or moderate dust loadings, with the largest response in the diurnal mode, but significant semidiurnal and Kelvin modes are present as well. We concentrate here on these three modes and on their sig-

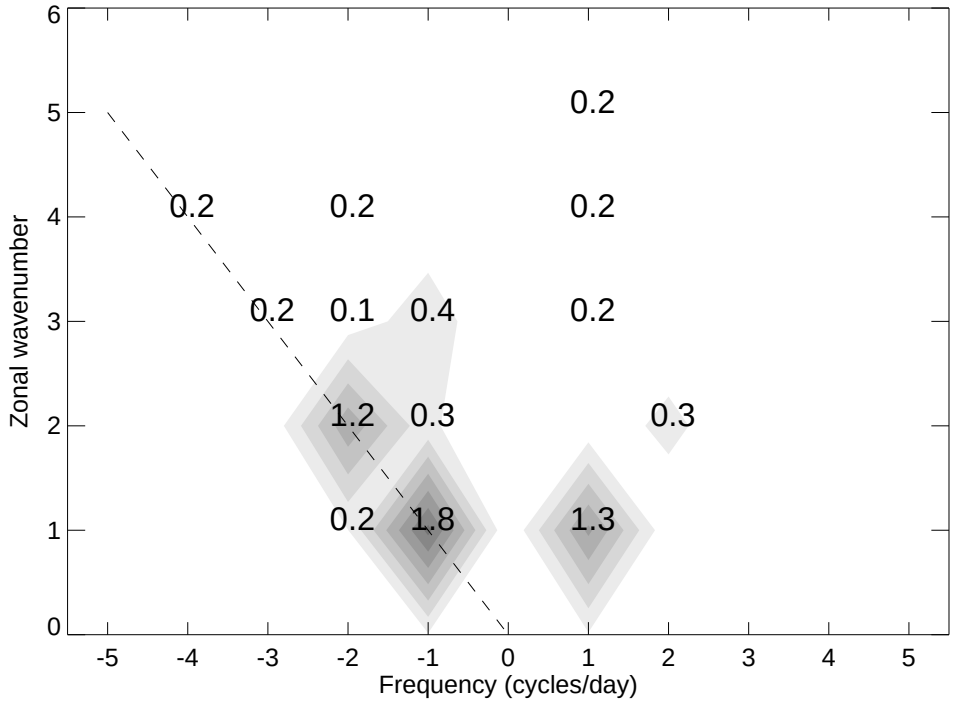

Fig. 1. Tidal mode amplitudes (as a percentage of the mean surface pressure) as a function of frequency and wavenumber from the Oxford MGCM at the equator averaged over $L_S = 240°$–$270°$, late northern hemisphere autumn. Negative frequency denotes a westward propagating mode and the dashed line indicates the Sun-synchronous modes. Modes with amplitudes greater than 0.1% are labelled, the grey-scale shading is at intervals of 0.25%.

nal in the surface pressure field, both for simplicity and for comparison with previous observations, although it is also desirable to investigate the tides' three-dimensional structure in the temperature and wind fields (e.g. Wilson and Hamilton, 1996; Bridger and Murphy, 1998; Wilson, 2000, 2002; Lewis and Read, 2003).

In this paper we first diagnose the thermal tides in a multiannual simulation using the Oxford MGCM, under prescribed dust conditions for reference, and then conduct a similar analysis on the output of the same model with assimilation of Mars Global Surveyor (MGS) Thermal Emission Spectrometer (TES) nadir temperature profiles and total dust opacities (Conrath et al., 2000; Smith et al., 2000, 2001) over the course of two Mars years. Mars Global Surveyor began mapping phase operations on 1 March 1999, $L_S = 104°$ of Mars Year (MY) 24, according to the Mars Year numbering scheme of Clancy et al. (2000). Routine nadir sounding retrievals were available for assimilation from $L_S = 140°$, MY 24 and the continuous assimilation period considered in this study extends to $L_S = 140°$, MY 26.

Data assimilation combines information from both present and past

observations using a GCM to produce a time-evolving analysis of the atmospheric state. With the advent of large atmospheric data sets from orbital missions such as MGS and developments in MGCMs, data assimilation for a planet other than the Earth is now possible. The scheme employed here is based on the analysis correction scheme (Lorenc et al., 1991), a form of successive corrections, which has proved simple and robust in trial studies with artificial data experiments under Martian conditions (Lewis and Read, 1995; Lewis et al., 1996, 1997).

In the case of the TES observations, the retrieved temperature profiles are assimilated in the form of layer thicknesses between pressure levels spaced one scale height ($\sim$ 10 km) apart in the lower atmosphere (0–40 km altitude). The model and observations are compared on this scale to avoid artificially smoothing small-scale structure present in the model which would not be seen in the nadir retrievals. Observations are repeatedly introduced to the model spread over a six hour time window and an empirically-determined horizontal correlation scale ($\sim$ 340–540 km), both weighted towards the correct time and location, in order to adjust the large-scale and slowly-varying components of the atmospheric flow. Velocity increments are also added, in thermal wind balance with the temperature adjustments. In the case of the dust observations, an additional quality control procedure is used to ensure that the data are not too noisy; this generally restricts observations to regions with a good thermal contrast between atmosphere and surface, in practice the afternoon over-pass (Smith et al., 2000). Dust opacity is measured by TES at 1075 cm^{-1} in the infrared, so the TES opacities are doubled as a conversion to the MGCM broadband visible opacity (visible opacity is assumed henceforth). There is no information about the vertical dust distribution in the lower atmosphere from the nadir observations, so the MGCM total opacity from ground to space is simply adjusted towards the TES observations by scaling the entire model dust profile. Further details of the TES assimilation are given in Lewis et al. (2005) and Montabone et al. (2005).

2 Tides in the MGCM

Figure 2 shows the amplitudes and phases of the three major tidal components, the diurnal and semidiurnal Sun-synchronous tides and the first Kelvin mode, over the course of two complete Mars years at the equator. The data begin and end around $L_S = 140^\circ$ to facilitate comparison with the assimilation results in the following section. The dust distribution for the MGCM was prescribed, and repeated exactly in each Mars year, based on a smoothed distribution representing background dust levels on Mars in the absence of dust storms. This had total optical depths typically of $\tau = 0.2$ at the equator and $\tau = 0.1$ at the poles, with a broad peak in dust up to $\tau = 0.5$ throughout the southern hemisphere

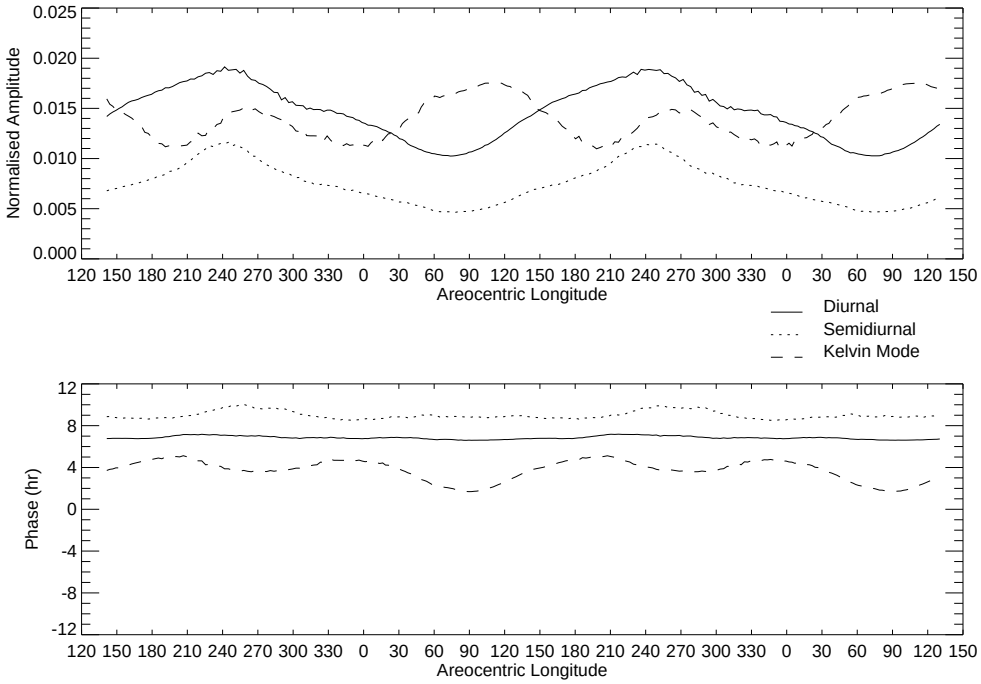

Fig. 2. Normalised amplitudes (upper panel) and phases (lower panel) at the equator for the three major modes over the course of two Mars years, chosen to match the assimilation period used later, from the Oxford MGCM run with a prescribed dust scenario, based on a repeated year without major dust storms. The diurnal and semidiurnal Sun-synchronous tides are shown with solid and dotted lines, and the first Kelvin mode with a dashed line. Phase is shown as the hour of first maximum with zero being midnight. Amplitudes and phases were calculated daily from the model output, but smoothed using a five day window for clarity.

and northern low latitudes during southern hemisphere spring and early summer. This prescribed dust distribution was found to give a good fit between the model and Mars Global Surveyor Radio Science temperature profiles under non-dust storm conditions (Read and Lewis, 2004), and forms a suitable basis for comparison here.

Over most of the year the diurnal tide is the largest single mode, with the semidiurnal tide evolving in a very similar pattern at about half the amplitude. Maxima in the Sun-synchronous tidal amplitudes occur around $L_S = 250°$, just before northern winter solstice ($L_S = 270°$) each year. At $L_S = 251°$, Mars is closest to the Sun and receives most Solar insolation, which, combined with the annual peak in dust levels, results in the strongest thermal forcing. The Kelvin mode might be expected to follow a similar pattern, as the result of an interaction between the diurnal mode and the surface topography, but in fact has two maxima per year, with the largest occurring during the relatively clear and cold northern hemisphere summer, when the

diurnal mode is small. This large response is most likely to be due to the first Kelvin mode frequency (1/sol) being close to atmospheric resonance under these conditions (Zurek, 1988) and has been previously reported in other MGCMs (e.g. Wilson and Hamilton, 1996; Bridger and Murphy, 1998).

A tidal heating rate which peaks at local noon would imply pressure maxima for the diurnal tide at 0600, and the semidiurnal tide at 0900 (and 2100), in the undamped case. According to classical tidal theory (Chapman and Lindzen, 1970), the temperature and pressure response is in quadrature with the local thermal forcing, in the absence of dynamics. Figure 2 shows that the diurnal westward tide phase is remarkably constant, at close to 0700 throughout the year, whereas the semidiurnal phase varies slightly between about 0900–1000. The Kelvin mode phase varies more, and tends to advance to earlier times when the amplitude of the response is greatest (at $L_S = 90°$), most notably around $L_S = 90°$. A similar advance in the phase of the total diurnal component of the Viking Lander surface pressure data has been observed at the same time of year and was interpreted as evidence of the presence of a Kelvin wave (Wilson and Hamilton, 1996). As noted earlier, the single-point lander observations cannot be separated into eastward and westward propagating modes.

Figure 3 illustrates the latitudinal structure of the same modes at northern hemisphere summer solstice, $L_S = 90°$. The maximum amplitude of the diurnal mode can be seen to be biased toward the northern hemisphere, where the heating is strongest, whereas the semidiurnal and Kelvin modes are more symmetric about the equator; in agreement with classical tidal theory, both are equatorially-trapped modes. It is notable that the phases are broadly constant with latitude in equatorial regions, except for a tendency for the diurnal phase to advance towards the south. The broad latitudinal structure and latitudinal phase invariance of the semidiurnal and Kelvin modes are defining features and consistent with structures shown by Wilson and Hamilton (1996) and Bridger and Murphy (1998). Large variations in the Sun-synchronous tidal phases mainly occur poleward of about 60° in each hemisphere where the tidal amplitudes are very small. It is worth noting that the diurnal mode can no longer propagate vertically more than 30° from the equator (Chapman and Lindzen, 1970). There are signs that the secondary maximum in the semidiurnal tide (around 2100) is being picked up by the analysis when the amplitude becomes very small and there is also the possibility of nonlinear coupling with planetary waves at high latitudes. The Kelvin mode has a remarkably constant phase at almost all latitudes.

3 Tides in the assimilation

Figure 4 now compares similar tidal mode diagnostics from the output of

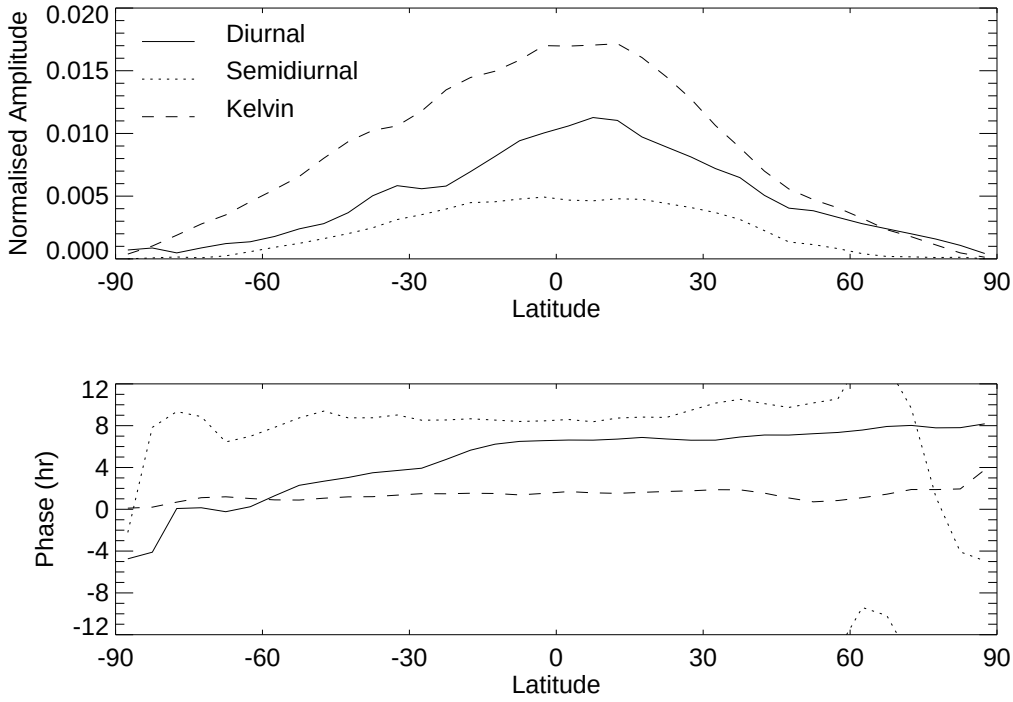

Fig. 3. The latitudinal structure of the normalised amplitude (upper panel) and phase (lower panel) of the diurnal, semidiurnal and Kelvin modes at $L_S = 90°$.

an assimilation of MGS TES thermal and total dust opacity observations from $L_S = 140°$, MY 24 to $L_S = 140°$, MY 26. Comparison with Fig. 2 immediately highlights the more irregular time dependence of the tides in the assimilation, influenced not only by the regular temperature profile observations but also by the updates to the dust opacity which is now longitudinally-asymmetric as well as time-dependent. It is notable that tidal amplitudes tend to be stronger in Fig. 4, which has a more variable and sometimes dustier atmosphere compared to the smoothly varying, zonally uniform, dust scenario used for Fig. 2.

Particular peaks in the tidal amplitude response indicate the presence of individual dust storm events. In MY 24 there is an indication of a tidal peak around $L_S = 225°$ and, to a lesser extent, following $L_S = 330°$, with a notable rapid growth in the Kelvin mode, as the diurnal Sun-synchronous tide grows, in both cases. The 2001 global dust storm (Smith et al., 2002) dominates MY 25, beginning around $L_S = 190°$, which is particularly clearly marked by the growth of the semidiurnal tidal amplitude. In contrast, the Kelvin mode is small during the height of the global dust storm, and there is no obvious sign of a resonant growth in the Kelvin mode during northern hemisphere summer, as was seen clearly in Fig. 2 and predicted by theory (Zurek, 1976, 1988), which indicates that the period of the first Kelvin mode for a clear atmosphere is close to one day. The dustier,

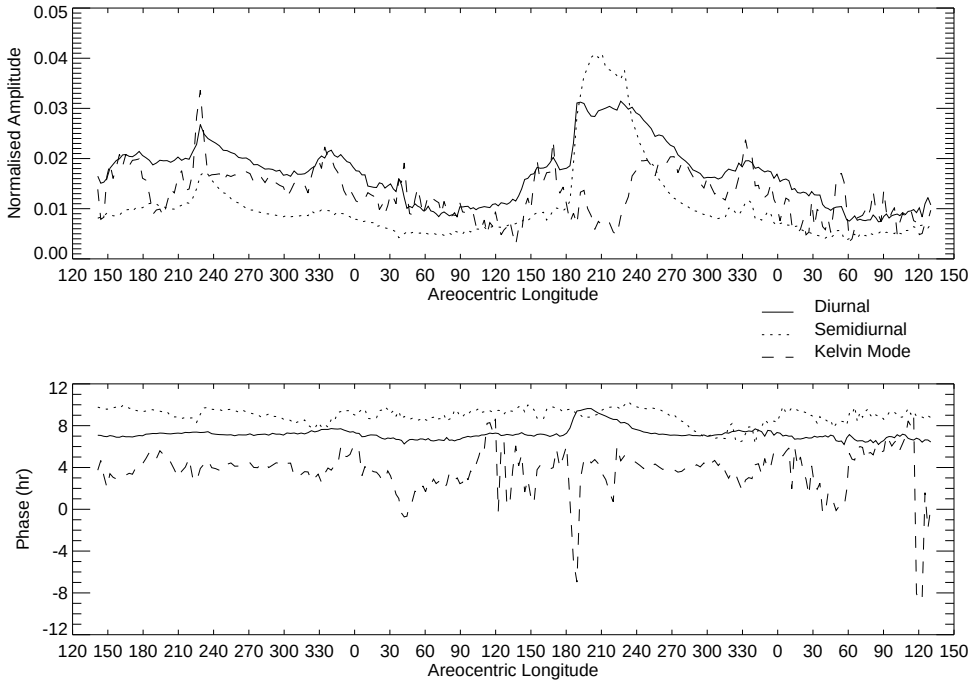

Fig. 4. As Fig. 2 (note that the amplitude scale has doubled), but based on results with data assimilation of TES thermal profiles and total dust opacities over the period $L_S = 140°$, MY 24 to $L_S = 140°$, MY 26.

and more disturbed, atmosphere in the assimilations does not permit as strong a resonance.

The phase information in Fig. 4 demonstrates the remarkable insensitivity of the phase of the Sun-synchronous diurnal tide to changes in dust loading and hence in its amplitude. The one clear change in phase occurs at $L_S = 190°$, MY 25, when the phase is retarded by more than two hours during the main period of the global dust storm. This change in phase may relate to increased solar absorption by dust higher in the atmosphere, compared to convective heating from the surface, and reflects the change in the altitude of the peak forcing by a significant fraction of the vertical wavelength of the diurnal mode (~ 30 km). There is no corresponding change in the phase of the semidiurnal mode at this time; its longer vertical wavelength (~ 100 km) means that the phase at the ground is insensitive to the altitude of the peak forcing in the lower atmosphere. The semidiurnal tide shows only small changes in phase, but there is some evidence of gradual advances in phase by about one hour, interrupted by the dust storm events at $L_S = 225°$ and $L_S = 330°$ in MY 24, and in the period following the global dust storm in MY 25. The large apparent phase shift in the Kelvin mode at $L_S = 190°$, MY 25, is probably associated with the rapid growth of the diurnal westward tide at the onset of the dust storm, and the longitu-

dinally asymmetric dust distribution at this time; other large phase variations appear at times when the Kelvin mode is relatively weak.

Figure 5 shows the assimilated dust loading averaged over the equatorial region and its correlation with tidal mode amplitudes; unlike Fig. 4, here plotted on a daily basis. Peaks in the dust loading are rapidly reflected in the diurnal westward tide, but the closest correlation is with the semidiurnal mode. The Pearson Correlation Coefficient for the dust and semidiurnal tidal amplitude, $r = 0.983$ (where $r = 1$ indicates a perfect linear relationship), reflects the remarkably linear relationship between the two. This is most apparent during the global dust storm in the second year, when the diurnal mode also grows, but appears to saturate at the storm's height. This is a result of the much longer vertical wavelength ($\sim 100\,\mathrm{km}$) of the semidiurnal tide, which effectively integrates solar absorption over the whole depth of the dust layer, compared to that of the diurnal tide ($\sim 30\,\mathrm{km}$), which may suffer destructive interference when the dust is mixed over comparable or greater height ranges. Thus the semidiurnal Sun-synchronous tide is preferentially forced when the heating is distributed over a number of atmospheric scale heights (Leovy and Zurek, 1979), as is observed on Mars (Zurek, 1981) and in the assimilation here. The peak amplitude of the semidiurnal tide in this analysis is comparable with the 4% normalised semidiurnal pressure amplitude seen at the Viking Lander 1 site following the 1977b global dust storm (Wilson and Hamilton, 1996, Fig. 2).

By comparison, the Pearson Correlation Coefficient for the dust and diurnal tidal amplitude is $r = 0.767$, and for the dust and Kelvin mode amplitude it is $r = 0.027$. There is a clear correlation between the dust loading and the amplitude of the diurnal, Sun-synchronous tide, as might be expected, but the relationship is less close to linear than it is in the case of the semidiurnal, Sun-synchronous tide. This is largely a result of the saturation of the diurnal tide at higher dust loadings. There is very little correlation between the Kelvin mode amplitude and the dust loading. In this case, higher dust loadings may enhance the strength of the tidal forcing, but, under dustier conditions, the period of the Kelvin mode is moved further from resonance with the diurnal tide, resulting in a reduced response to that forcing.

4 Conclusions

This study has illustrated a benefit of data assimilation in its ability to combine information from different observations and to produce a full, physically-consistent global analysis of all atmospheric fields, including those not directly observed, in this case surface pressure. The TES instrument is primarily able to observe two phases of the tides in mid- and low-latitudes because of the Sun-synchronous nature of the MGS orbit, which crosses the equator around 2am/2pm local time. Providing a best fit to the tides where thermal

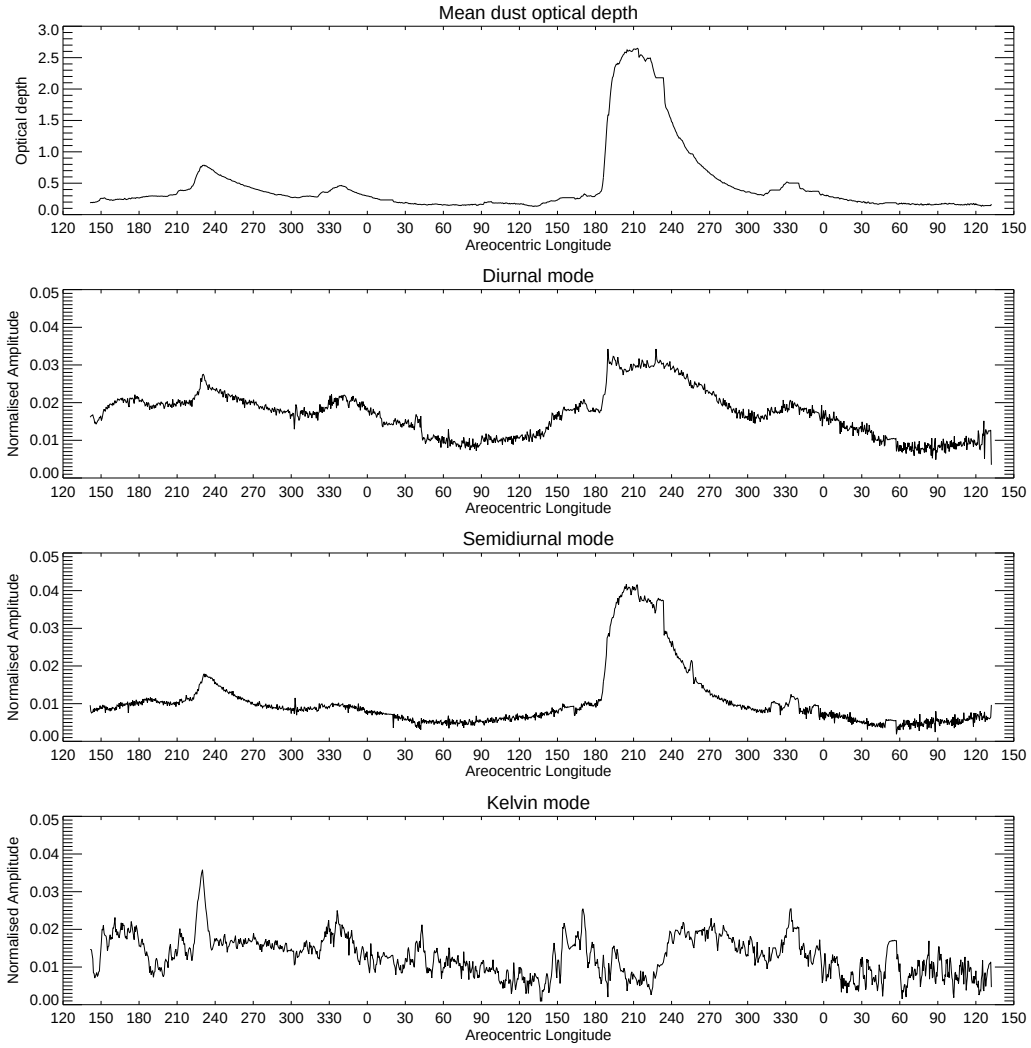

Fig. 5. The mean dust opacity in the region 30°S–30°N (upper panel), converted to the equivalent visible optical depth at 610 Pa, for the assimilation period $L_S = 140°$, MY 24 to $L_S = 140°$, MY 26. The three panels below show the amplitudes of the diurnal, semidiurnal and Kelvin modes respectively. Unlike Fig. 4, these are plotted for the daily calculations with no smoothing.

data are available, and including further information by updating the dust distribution, which in turn impacts the solar forcing calculated by the model, permits an analysis of the total tidal modes consistent with the observations available. The global nature and regular sampling possible with output from assimilation also has advantages compared to direct analysis of single-point surface observations, where it is possible to diagnose the amplitudes of tides at various periods but not to distinguish unambiguously between eastward and westward propagating components.

Having said this, clearly *in situ* observations would be invaluable for validation of the results. The unfortunate loss of the ESA Beagle 2 mission,

and the lack of meteorological sensors aboard the NASA Mars Exploration Rovers, means that the ideal scenario of simultaneous satellite and lander observations is not possible at present.

References

Banfield, D., Conrath, B. J., Smith, M. D., Christensen, P. R., Wilson R. J., 2003. Forced waves in the Martian atmosphere from MGS TES nadir data. Icarus 161, 319-345.

Bridger, A. F. C., Murphy, J. R., 1998. Mars' surface pressure tides and their behavior during global dust storms. J. Geophys. Res. 103, 8587-8601.

Chapman, S., Lindzen, R. S., 1970. Atmospheric Tides. Reidel, Dordrecht, Netherlands.

Clancy, R. T., Sandor, B. J., Wolff, M. J., Christensen, P. R., Smith, M. D., Pearl, J. C., Conrath, B. J., Wilson, R. J., 2000. An intercomparison of ground-based millimeter, MGS TES, and Viking atmospheric temperature measurements: Seasonal and interannual variability of temperature and dust loading in the global Mars atmosphere. J. Geophys. Res. 105, 9553–9572.

Conrath, B. J., 1976. Influence of planetary-scale topography on the diurnal thermal tide during the 1971 Martian dust storm. J. Atmos. Sci. 33, 2430–2439.

Conrath, B. J., Pearl, J. C., Smith, M. D., Maguire, W. C., Dason, S., Kaelberer, M. S., Christensen, P. R., 2000. Mars Global Surveyor Thermal Emission Spectrometer (TES) observations: Atmospheric temperatures during aerobraking and science phasing. J. Geophys. Res. 105 (E4), 9509–9519.

Forbes, J. M., Bridger, A. F. C., Bougher, S. W., Hagan, M. E., Hollingsworth, J. L., Keating, G. M., Murphy, J., 2002. Nonmigrating tides in the thermosphere of Mars. J. Geophys. Res. 107, 5113, doi:10.1029/2001JE001582.

Hess, S. L., Henry, R. M., Leovy, C. B., Ryan, J. A., Tillman, J. E., 1977. Meteorological results from the surface of Mars: Viking 1 and 2. J. Geophys. Res. 82, 4559–4574.

Leovy, C. B., 1981. Observations of Martian tides over two annual cycles. J. Atmos. Sci. 38, 30–39.

Leovy, C. B., Zurek, R. W., 1979. Thermal tides and Martian dust storms: Direct evidence for coupling. J. Geophys. Res. 84, 2956–2968.

Lewis, S. R., Collins, M., Read, P. L., 1996. Martian atmospheric data assimilation with a simplified general circulation model: Orbiter and lander networks. Plan. Space Sci. 44, 1395–1409.

Lewis, S. R., Collins, M., Read, P. L., 1997. Data assimilation with a Martian atmospheric GCM: An example using thermal data. Adv. Space Res. 19(8), 1267–1270.

Lewis, S. R., Read, P. L., 1995. An operational data assimilation scheme for the Martian atmosphere. Adv. Space Res. 16(6), 9–13.

Lewis, S. R., Read, P. L., 2003. Equatorial jets in the dusty Martian atmosphere.

J. Geophys. Res. 108 (E4), doi:10.1029/2002JE001933.

Lewis, S. R., Read, P. L., Conrath, B. J., Pearl, J. C., Smith, M. D., 2005. Assimilation of Thermal Emission Spectrometer atmospheric data during the Mars Global Surveyor aerobraking period. Icarus, submitted.

Lindzen, R. S., 1970. The application and applicability of terrestrial atmospheric tidal theory to Venus and Mars. J. Atmos. Sci. 27, 536–549.

Lorenc, A. C., Bell, R. S., Macpherson, B., 1991. The Meteorological Office analysis correction data assimilation scheme. Quart. J. R. Meteor. Soc. 117, 59–89.

Montabone, L., Lewis, S. R., Read, P. L., 2005. Interannual variability of Martian dust storms in assimilation of several years of Mars Global Surveyor observations. Adv. Space Res., this issue.

Read, P. L., Lewis, S. R., 2004. The Martian Climate Revisited: Atmosphere and Environment of a Desert Planet. Springer-Verlag, Berlin, ISBN: 3-540-40743-X.

Smith, M. D., Pearl, J. C., Conrath, B. J., Christensen, P. R., 2000. Mars Global Surveyor Thermal Emission Spectrometer (TES) observations of dust opacity during aerobraking and science phasing. J. Geophys. Res. 105 (E4), 9539–9552.

Smith, M. D., Pearl, J. C., Conrath, B. J., Christensen, P. R., 2001. Thermal Emission Spectrometer results: Mars atmospheric thermal structure and aerosol distribution. J. Geophys. Res. 106 (E4), 23929–23945.

Smith, M. D., Conrath, B. J., Pearl, J. C., Christensen, P. R., 2002. Thermal Emission Spectrometer observations of Martian planet-encircling dust storm 2001a. Icarus 157, 259–263.

Wilson, R. J., 2000. Evidence for diurnal period Kelvin waves in the Martian atmosphere from Mars Global Surveyor TES data. Geophys. Res. Lett. 27, 3889–3892.

Wilson, R. J., 2002. Evidence for nonmigrating thermal tides in the Mars upper atmosphere from the Mars Global Surveyor accelerometer experiment. Geophys. Res. Lett. 29(7), doi:10.1029/2001GL013975.

Wilson, R. J., Hamilton, K., 1996. Comprehensive model simulation of thermal tides in the Martian atmosphere. J. Atmos. Sci. 53, 1290–1326.

Zurek, R. W., 1976. Diurnal tide in the Martian atmosphere. J. Atmos. Sci. 33, 321–337.

Zurek, R. W., 1981. Inference of dust opacities for the 1977 Martian great dust storms from Viking Lander 1 pressure data. Icarus 45, 202–215.

Zurek, R. W., 1988. Free and forced modes in the Martian atmosphere. J. Geophys. Res. 93, 9452–9462.

Zurek, R. W., Leovy, C. B., 1981. Thermal tides in the dusty Martian atmosphere: A verification of theory. Science 213, 437–439.

Zurek, R. W., Barnes, J. R., Haberle, R. M., Pollack, J. B., Tillman, J. E., Leovy, C. B., 1992. Dynamics of the atmosphere of Mars. In: Kieffer, H. H., Jakosky, B. M., Snyder, C. W., Matthews, M. S. (Eds.), Mars. University of Ari-

zona Press, Tucson, pp. 835–933.